NMR structure reveals intramolecular regulation mechanism for pheromone binding and release

Reto Horst*, Fred Damberger*, Peter Luginbühl*, Peter Güntert*, Guihong Peng†, Larisa Nikonova†, Walter S. Leal†‡, and Kurt Wüthrich*§

*Institut für Molekularbiologie und Biophysik, Eidgenössische Technische Hochschule, CH-8093 Zürich, Switzerland; †National Institute of Agrobiological Sciences, Tsukuba, Ibaraki 305-8634, Japan; and ‡Department of Entomology, University of California, Davis, CA 95616

Contributed by Kurt Wüthrich, October 8, 2001

Odorants are transmitted by small hydrophobic molecules that cross the aqueous sensillar lymph surrounding the dendrites of the olfactory neurons to stimulate the olfactory receptors. In insects, the transport of pheromones, which are a special class of odorants, is mediated by pheromone-binding proteins (PBPs), which occur at high concentrations in the sensillar lymph. The PBP from the silk moth *Bombyx mori* (BmPBP) undergoes a pH-dependent conformational transition between the forms BmPBP^A present at pH 4.5 and BmPBP^B present at pH 6.5. Here, we describe the NMR structure of BmPBP^A, which consists of a tightly packed arrangement of seven α-helices linked by well defined peptide segments and knitted together by three disulfide bridges. A scaffold of four α-helices that forms the ligand binding site in the crystal structure of a BmPBP–pheromone complex is preserved in BmPBP^A. The C-terminal dodecapeptide segment, which is in an extended conformation and located on the protein surface in the pheromone complex, forms a regular helix, α_7, which is located in the pheromone-binding site in the core of the unliganded BmPBP^A. Because investigations by others indicate that the pH value near the membrane surface is reduced with respect to the bulk sensillar lymph, the pH-dependent conformational transition of BmPBP suggests a novel physiological mechanism of intramolecular regulation of protein function, with the formation of α_7 triggering the release of the pheromone from BmPBP to the membrane-standing receptor.

Male moths have an exquisitely sensitive olfactory system capable of detecting over great distances single molecules of pheromones emitted by the female, and they are capable of distinguishing highly selectively between closely similar compounds or isomers (1). These capabilities of male moths are because of olfactory sensory organs that consist of large branched antennae and can readily be isolated for biochemical characterization or electrophysiological recordings (2). The surface of the antennae is covered with hairlike protrusions composed of cuticle, which form a sheath (sensillum) surrounding one or several dendrite endings from olfactory neurons. The dendrites in each sensillum are bathed in a special fluid, the sensillum lymph. Odorant molecules gain access to the dendritic membrane through pores penetrating the sensillum wall and then crossing the sensillar lymph to interact with G protein-coupled olfactory receptors, which form a large eukaryotic protein family. Upon interaction with the olfactory receptors, a cascade of events leads to a change of the membrane potential (3), resulting in opening of ion channels and depolarization.

Common odorants are hydrophobic molecules that are poorly soluble in aqueous media, such as the sensillar lymph. Odorants overcome this barrier by binding to odorant-binding proteins (OBPs). OBPs are present at high concentrations in the lymph (up to 10 mM), bind the odorant, and transport it from the sensillum pore wall to the receptor at the dendritic membrane. It is not known whether the receptor recognizes either the odorant–OBP complex or the free odorant after its release by the OBP (4). A number of authors have proposed that OBPs might play an active role in odorant recognition, either by preferential binding of certain ligands or by forming odorant–OBP complexes with distinctive conformations that would support recognition of specified odorants by the receptor (5). Support for this hypothesis has been derived from the fact that a large number of different OBPs are usually isolated from an individual species, but that only one type of OBP is typically found in a given sensillum (6).

OBPs are small, highly water-soluble acidic proteins ranging from 14 to 16 kDa in size, which have been identified in many insect species and represent two different protein families. Pheromone-binding proteins (PBPs) are isolated from sensilla that are responsive specifically to pheromones produced by the females, whereas general OBPs have been found in sensilla that respond to a range of plant volatiles and odorants originating from food sources. Within a given species, several different

Table 1. Input of conformational constraints and structure calculation for BmPBP^A with the programs DYANA and OPAL

Quantity	Value
NOE upper distance restraints	2,109
Intraresidual	857
Sequential	451
Medium range	384
Long range	417
Dihedral angle constraints	478
DYANA target function value (Å^2)*†	1.3 ± 0.2 (0.7–1.5)
Residual NOE distance constraint violations*	
Number > 0.1 Å	31 ± 4 (24–38)
Sum (Å)	25.3 ± 0.9 (23.3–27.3)
Maximum (Å)	0.15 ± 0.01 (0.13–0.17)
Rms deviations (rmsd) (Å)*‡	
Backbone (8–142)	0.46 ± 0.07 (0.38–0.62)
Heavy atoms (8–142)	0.78 ± 0.06 (0.7–0.92)
Ramachandran plot statistics§	
Most favored regions (%)	83.8
Additional allowed regions (%)	15.5
Generously allowed regions (%)	0.7
Disallowed regions (%)	0

*The number given is the average ± the standard deviation for the set of 20 energy-refined conformers used to represent the NMR structure, with minimum and maximum values given in parentheses.
†Before energy minimization.
‡rmsd values are relative to the mean coordinates.
§As determined by PROCHECK (29).

Abbreviations: OBP, odorant-binding protein; PBP, pheromone-binding protein; BmPBP, *B. mori* pheromone-binding protein; NOE, nuclear Overhauser effect; NOESY, NOE spectroscopy; rmsd, rms deviation.

Data deposition: The atomic coordinates have been deposited in the Protein Data Bank, www.rcsb.org (PDB ID code 1GM0).

§To whom reprint requests should be addressed. Fax: +4116331151.

The publication costs of this article were defrayed in part by page charge payment. This article must therefore be hereby marked "*advertisement*" in accordance with 18 U.S.C. §1734 solely to indicate this fact.

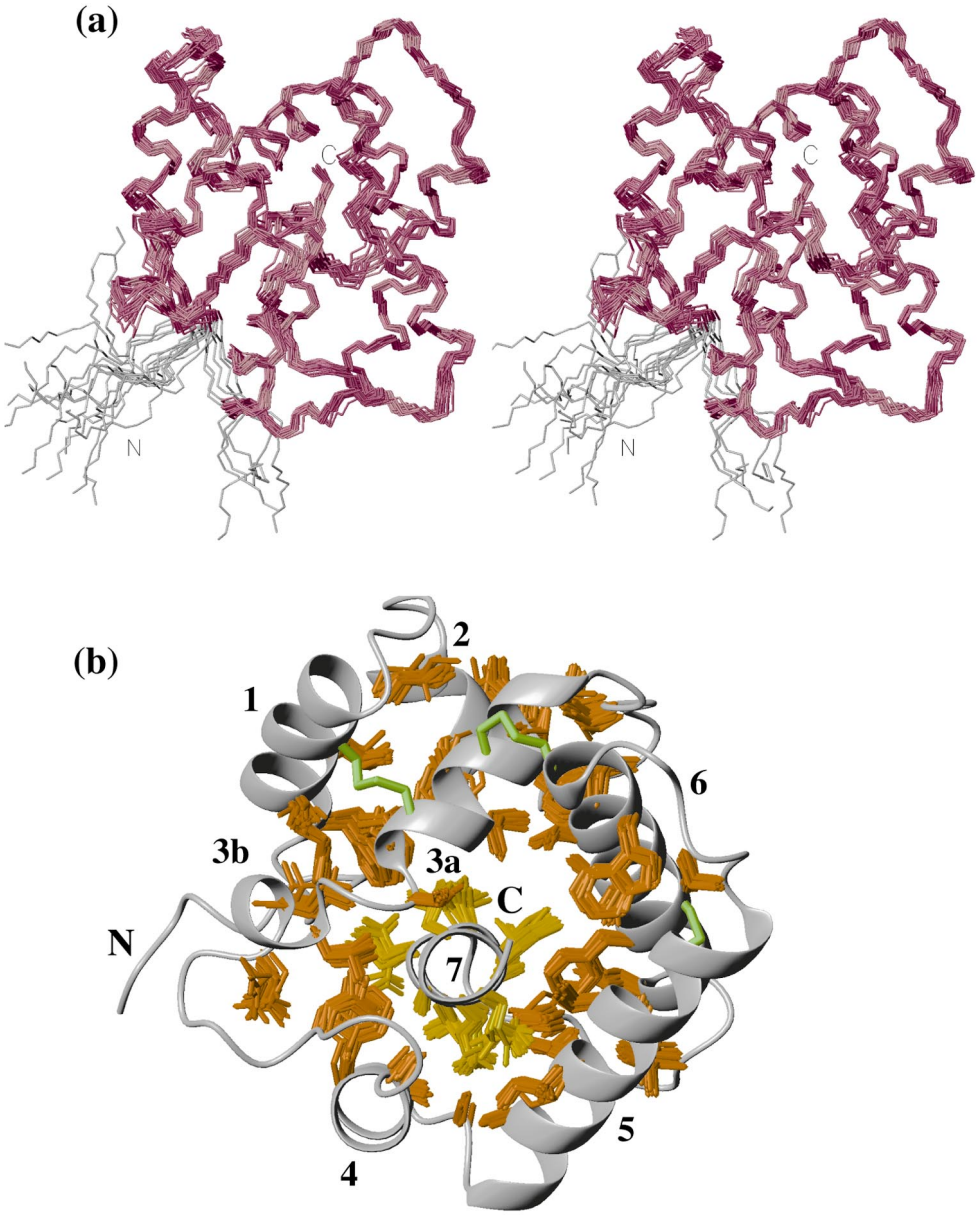

Fig. 1. Structure of BmPBP^{A}. (*a*) A stereo view of the polypeptide backbone fold of the NMR structure of BmPBP^{A} represented by a bundle of 20 energy-minimized DYANA conformers. The superposition is for minimal rmsd of the backbone heavy atoms of residues 8–142 (magenta). The disordered residues 1–7 are indicated in gray. The chain ends are identified by the letters N and C. (*b*) Ribbon drawing of one of the 20 energy-minimized conformers, which was obtained after a rotation by about 90° relative to the orientation shown in *a*. The structure contains seven α-helices (see the text and Fig. 2 for the notation α_{3a} and α_{3b}) that are connected by linkers with nonregular secondary structure. The sequential order of the α-helices is indicated by the numbers 1 to 7, and the N and C termini are identified. The 53-aa side chains with solvent-accessible surface area below 15%, which form the hydrophobic core of the protein, are shown as bundles of 20 conformers, similar to the presentation in *a*. All but the first residue of helix α_7 belong to this group and are indicated in yellow, whereas the other solvent-inaccessible side chains are drawn in red. The three disulfide bridges Cys-19–Cys-54, Cys-50–Cys-108, and Cys-97–Cys-117 are drawn in green for one of the 20 conformers. This and all other figures showing molecular models of BmPBP were generated with the program MOLMOL (26).

general OBPs and one or several PBPs are typically identified. Sequence alignments reveal that six cysteines are strictly conserved in all OBPs. In moth species, the mature form of OBPs is 142 aa in length. Recently, it was demonstrated by NMR spectroscopy in solution that the PBP from the moth species *Bombyx mori* (BmPBP) undergoes a pH-dependent conformational transition (7). Above pH 6.0, BmPBP occurs in a basic form (BmPBP^{B}), whereas below pH 4.9 an acidic form (BmPBP^{A}) is observed. In the pH range of 4.9–6.0, a mixture of the A and B forms exists, which is in slow exchange on the NMR time scale.

Conformational heterogeneity observed in other OBPs indicates that pH-dependent conformational polymorphism may be a common feature of these proteins. This and the observation that a number of OBPs, including BmPBP, do not bind ligands below pH 5.0 (8, 9) suggests that pH variation of the folded conformation might play a physiological role in olfaction (10, 11). In this context, it is intriguing that near-UV circular dichroism measurements revealed that BmPBP undergoes a conformational transition when mixed with model membranes (12). Thus, as BmPBP approaches the dendritic membrane, it might undergo a conformational change to the BmPBP^{A} form (7, 13) and thus trigger the release of the ligand to the receptor.

The structure of BmPBP in a complex with bombykol, which is a pheromone component emanated by female *B. mori*, was determined by x-ray crystallography in crystals grown at pH 8.2 (14). BmPBP in this complex with bombykol consists of six α-helices, which are knitted together by three disulfide bonds and completely surround the ligand, so that bombykol is protected from the aqueous solvent by a hydrophobic binding pocket. Sandler *et al.* (14) propose either that a loop covering the pheromone-binding pocket may move aside to allow entry of the ligand or that the entire protein may partially unfold to allow entry of the ligand, as there is no obvious entrance or exit for the ligand in the structure of the complex. To obtain more insight into the mechanisms of ligand binding and release, and the role played by the pH-dependent conformational transition in OBPs, we have started a project of NMR structure determination for all of the different conformations of BmPBP that seem to have a role in its physiological function. Here, we present the solution

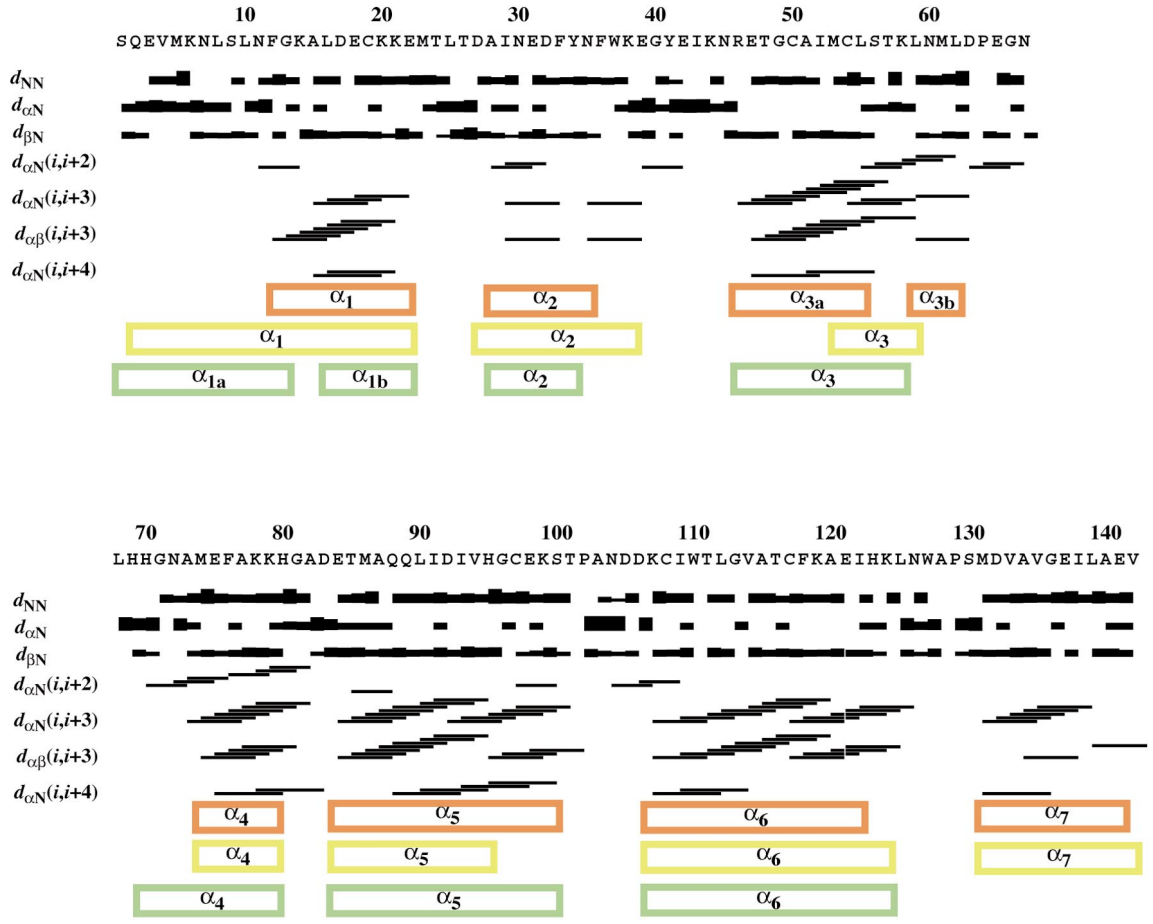

Fig. 2. Secondary structure information from sequential and medium-range NOEs for BmPBP^A. The sequential NOE connectivities are indicated with thick or thin lines for strong or weak NOEs, respectively. The medium-range connectivities are shown by lines starting and ending at the positions of the residues related by the NOE. The locations of α-helices in BmPBP^A are indicated by red boxes, the helical regions predicted by the secondary structure prediction program PHDsec (23) from the BmPBP amino acid sequence by yellow boxes, and the α-helices in the crystal structure of a BmPBP–bombykol complex (14) by green boxes. We have chosen the notations α_{1a} and α_{1b} for the BmPBP–bombykol complex and α_{3a} and α_{3b} for BmPBP^A because of the overlap with α_1 and α_3 in the other two data sets.

structure of the acidic form observed at pH 4.5, BmPBP^A (7, 13), which reveals a striking conformational difference to the BmPBP conformation in the crystal structure of the bombykol complex. The C-terminal segment consisting of residues 131–141, which is in an extended conformation and located on the protein surface in the BmPBP–bombykol complex, forms an α-helix that is located in the protein core in BmPBP^A. This suggests a novel intramolecular regulation mechanism of protein function by major conformational rearrangements involving residues that are widely separated in the amino acid sequence.

Materials and Methods

Sample Preparation. The expression and purification of $^{13}C,^{15}N$-labeled BmPBP in *Escherichia coli* has been described (7). The NMR sample used for the structure determination of BmPBP^A was prepared by redissolving 9.75 mg of $^{13}C,^{15}N$-labeled BmPBP lyophilized from H_2O solution in 95% H_2O/5% D_2O containing 50 mM potassium phosphate buffer at pH 4.5 and 2 mM NaN_3, resulting in $\approx$1 mM protein concentration.

NMR Data Collection and Structure Calculation. All NMR data recorded to obtain structural constraints (Table 1) were performed at a ^1H frequency of 750 MHz on a Bruker DRX 750 spectrometer at 20°C. Distance constraints were obtained from three nuclear Overhauser effect spectroscopy (NOESY) experiments with mixing times of 50 ms, i.e., a three-dimensional ^{15}N-resolved [^1H,^1H]-NOESY spectrum and two three-dimensional ^{13}C-resolved [^1H,^1H]-NOESY spectra with the ^{13}C carrier frequency in the aliphatic and aromatic region, respectively. The three data sets were interactively peak-picked by using the program XEASY (15), and the peaks were automatically integrated by using SPCSAN (Ralf Glaser, personal communication), resulting in 4,653 NOE cross-peak intensities. On the basis of the BmPBP^A sequence-specific resonance assignments (16), NOE cross-peak assignments were then obtained by using the module CANDID (T. Hermann, P.G., and K.W., unpublished data) within the program DYANA (17). CANDID/DYANA performs automated assignment and distance calibration of NOE intensities, removal of "meaningless" NOE distance constraints, and automatic NOE upper distance limit violation analysis. The CANDID/DYANA calculation consisted of seven cycles of iterative NOE assignment and structure calculation. During the first six CANDID cycles, ambiguous distance constraints (18) were used. For the final structure calculation, only distance constraints were retained that corresponded to unambiguously assigned NOE cross-peaks after the sixth CANDID cycle, resulting in 2,109 upper distance constraints; 478 torsion angle constraints obtained from short-range NOE data by using the module FOUND (19) were added in the last calculation. Energy refinement of the resulting DYANA conformers was done in a water shell with the program OPALP (20, 21), using the AMBER force field (22).

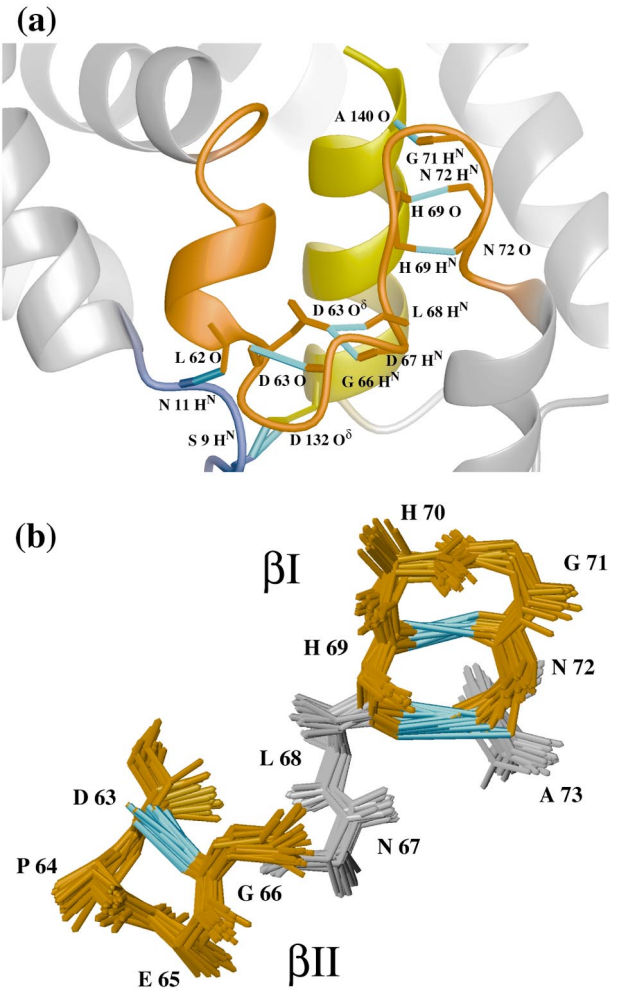

Fig. 3. Two close-up views of features in BmPBP^{A} that differ from the conformation of the corresponding polypeptide segments in the crystal structure of a BmPBP–bombykol complex (14). (*a*) Surroundings of the C-terminal helix α_7. The peptide segment linking α_{3a} and α_4 (residues 56–73), which includes the helix α_{3b}, is indicated in orange, the residues 9–11 in blue, and the helix α_7 with residues 131–142 in yellow. Hydrogen bonds identified in the loop region are indicated in cyan. (*b*) Close-up view of the loop region of residues 63–73, represented by a bundle of 20 energy-minimized DYANA conformers. The backbone heavy atoms, H^N and C^β, have been locally superimposed for best fit, yielding a backbone rmsd for this region of 0.4 Å. A type II β turn of residues 63–66 and a type I β turn of residues 69–72 are indicated in orange, and the remaining residues are shown in gray. The hydrogen bonds are drawn in cyan.

Results and Discussion

NMR Structure of BmPBP^{A}. The A form of the 142-residue protein BmPBP consists of a tightly packed arrangement of seven α-helices consisting of the residues 12–22 (α_1), 28–35 (α_2), 46–55 (α_{3a}),74–79 (α_4), 84–100 (α_5), 107–122 (α_6), and 131–141(α_7) (Fig. 1*b*). The N-terminal peptide segment of residues 1–7 is flexibly disordered (Fig. 1*a*). The peptide segments linking the helices are well defined (Fig. 1*a*) but have no regular secondary structure, except for the four-residue helix α_{3b} in the 19-residue loop between α_{3a} and α_4. We use the notation α_{3a} and α_{3b} because of the overlap of these two helical structures with α_3 in the crystal structure of a BmPBP–bombykol complex as well as with the third helix obtained from sequence-based secondary structure prediction with the program PHDsec (23) (Fig. 2). A prominent feature of the structure is the location of the C-terminal helix α_7 in the hydrophobic core (Fig. 1*b*). The helix α_7 is framed by the four helices α_{3a}, α_4, α_5, and α_6 and is covered by the loop of residues 56–73 that connects the helices α_{3a} and α_4 and includes the short helix α_{3b} (Fig. 3*b*). The positioning of α_7 in BmPBP^{A} is determined by a dense network of more than 100 long-range NOEs between protons of all residues in the helix α_7 and protons of 26 residues located in the helices α_3, α_4, α_5, and α_6 (Fig. 4*a*). Overall, BmPBP^{A} thus has a well defined tertiary structure, which is in contrast to previous suggestions that BmPBP was unfolded at pH = 4.5 (12).

The C^β chemical shifts of the six cysteinyl residues are equal to or larger than 35 ppm (16), showing that all of the cysteines are oxidized (24). The disulfide bonds determined chemically (25) are consistent with the network of NOE distance constraints. The three-dimensional arrangement of the helices is anchored by the three disulfide bonds as well as by a large number of noncovalent hydrophobic contacts. Two disulfide bonds, Cys-19–Cys-54 and Cys-50–Cys-108, anchor the relative positions of the helices α_1, α_{3a} and α_5, and the third disulfide bond, Cys-97–Cys-117, connects α_5 with α_6 (Fig. 1*b*).

The conformation of the loop linking the helices α_{3a} and α_4 is defined by a dense network of long-range and medium-range NOE constraints, and hydrogen bonds were detected that stabilize its conformation (Fig. 3). The first half of the loop with residues 63–66 contains a classic type II β turn with a standard $i,i+3$ hydrogen bond, Gly-66 H^N–Asp-63 O (Fig. 3*b*), as well as two backbone–side chain hydrogen bonds, Asn-67 H^N–Asp-63 $O^{\delta 1}$ and Leu-68 H^N–Asp-63 $O^{\delta 1}$ (Fig. 3*a*). A type I β turn is formed by the residues 69–72, which cover the C-terminal end of helix α_7. This β turn is defined by the two hydrogen bonds His-69 H^N–Asn-72 O and Asn-72 H^N–His-69 O (Fig. 3*b*), and its position relative to the helix α_7 is fixed by a third hydrogen bond, Gly-71 H^N–Ala-140 O (Fig. 3*a*).

Two features highlighted in Fig. 3*a* show local differences between BmPBP^{A} and the protein conformation in the crystal structure of the BmPBP–bombykol complex (14). First, the N-terminal part of the α_1 helix seen in the crystal structure is replaced by an extended conformation in the NMR structure of BmPBP^{A}, with long-range hydrogen bonds to the helices α_{3b}, Asn-H^N 11–Leu-62 O, and α_7, Ser-9 H^N–Asp-132 $O^{\delta 1}$ and Ser-9 H^N–Asp-132 $O^{\delta 2}$. Second, in BmPBP^{A}, the peptide segment corresponding to the C-terminal turn of the helix α_3 in the crystal structure is replaced by a kinked turn connecting α_{3a} and α_{3b}, which has not been identified as part of a regular helical structure by the program MOLMOL (26).

The molecular surface of BmPBP^{A} contains 14 glutamates, nine aspartates, 14 lysines, and one arginine, which are all charged at pH 4.5, and there are no hydrophobic patches on the surface. This surface structure provides a rationale for the observation that BmPBP is highly soluble and monomeric in aqueous media at physiological concentrations and low pH (12).

Helix α_7 Fills the Binding Site of BmPBP. The differences between the protein conformations in the unliganded solution structure of BmPBP^{A} and the crystal structure of the BmPBP–bombykol complex (14) are most pronounced in the region of helix α_1, which is N-terminally elongated in the structure of the complex (helix α_{1a}), and in the C-terminal helix α_7, which is present only in BmPBP^{A} but has been indicated also by secondary structure prediction with the program PHDsec (23) (Fig. 2). The four helices α_1, α_3, α_5, and α_6 form the bombykol-binding cavity of the protein in the structure of the complex and occur in closely similar positions in BmPBP^{A}. In the corresponding segments of α_{1b}, α_{3a}, α_5, and α_6 in the two structures, the backbone atoms can be superimposed with an rmsd of 1.1 Å, and superposition of only the backbone atoms of α_{3a}, α_5, and α_6 results in an even better fit, with an rmsd of 0.6 Å. The most exciting observation is that the helix α_7 in the hydrophobic core of BmPBP^{A} (Fig. 1*b*) occupies a position that corresponds to the pheromone-binding

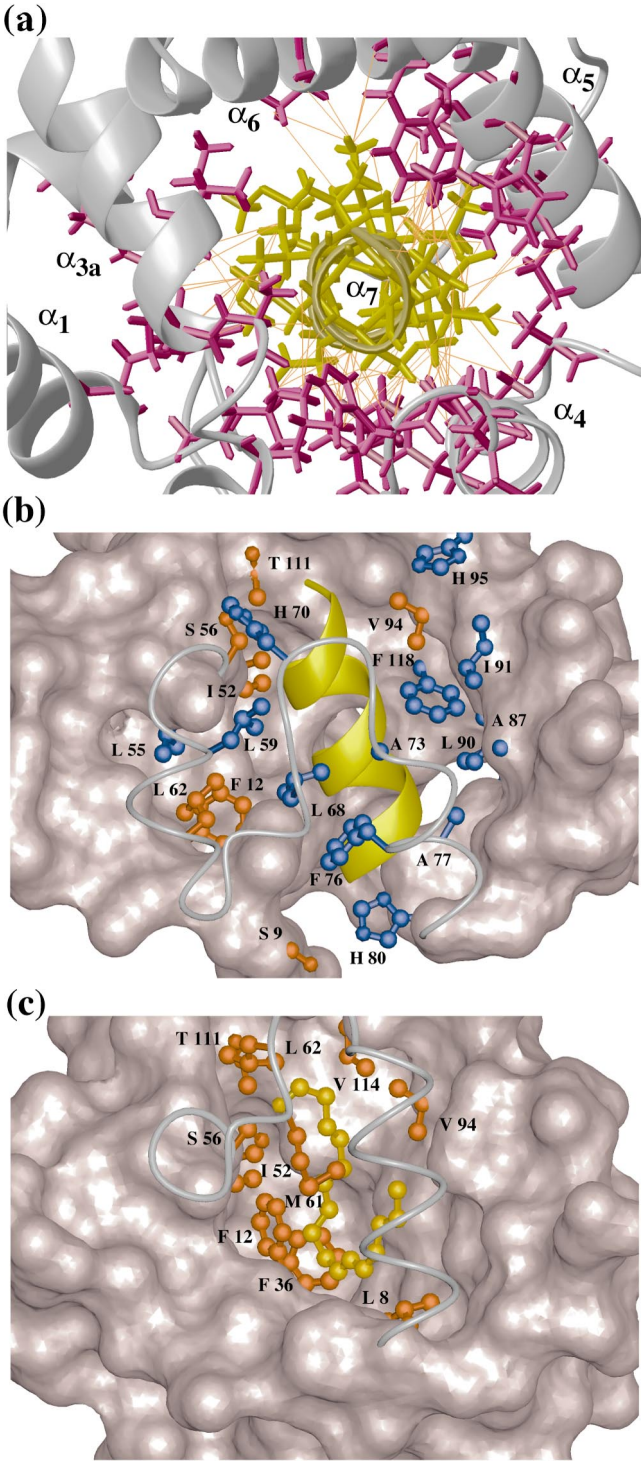

Fig. 4. Close-up views of the pheromone-binding site in a BmPBP–bombykol complex (14) and the corresponding molecular region of unliganded BmPBP^A. (*a*) NOE network in the potential ligand-binding region in BmPBP^A, viewed in the direction of the axis of the helix α_7 (same viewing angle as in Fig. 1*b*). In total, 125 upper-distance limits between residues of α_7 and the rest of the protein (shown in orange) define the position of α_7 in the core of BmPBP^A. α_7 is shown in yellow, side chains from the remainder of the protein are magenta, and the backbone is gray. (*b*) View of the hydrophobic core of BmPBP^A in a direction perpendicular to the axis of helix α_7. The bottom of the cavity, with this viewing angle, is drawn as a space-filling surface. The cover of the cavity formed by residues 56–79 is drawn by a gray line representing the polypeptide backbone. The C-terminal helix α_7 is represented by a yellow ribbon. Side chains that have heavy atoms within a distance of 4.0 Å to any atom in helix α_7 are drawn as ball-and-stick models. Among these, the side chains that also show contacts to bombykol in the crystal structure of the BmPBP–bombykol complex are highlighted in red, whereas the other drawn side chains are blue. (*c*) Similar presentation as *b* of the crystal structure of the BmPBP–bombykol complex. The side chains that have heavy atoms closer than 4.0 Å to any pheromone atom are drawn in red (Ser-9 is not visible). The pheromone is drawn as a gold-colored ball-and-stick-model. Comparison of *b* and *c* shows particularly clearly that the position of the helix α_7 in BmPBP^A corresponds to the location of the pheromone in the structure of the BmPBP–bombykol complex described by Sandler *et al.* (14).

site in the crystal structure of the BmPBP–bombykol complex (Fig. 4). Of the 20 residues in the A form that show contacts to helix α_7 (Fig. 4*b*), the seven residues Ser-9, Phe-12, Ile-52, Ser-56, Leu-62, Val-94, and Thr-111 also show contacts to the pheromone in the crystal structure of the BmPBP–bombykol complex. Of these seven residues, Phe-12, Ile-52, Ser-56, and Val-94 are highly conserved among lepidopteran OBPs, which independently supports that they may be important for the mechanism of pheromone binding and release. The three residues Leu-8, Phe-36, and Met-61, which show direct contacts to bombykol in the crystal structure of the BmPBP–bombykol complex (Fig. 4*c*), do not contact helix α_7 in the solution structure of the A form. Among these, Leu-8 and Phe-36 are highly conserved in lepidopteran OBPs, whereas position 61 shows little conservation across this class of proteins.

A Mechanism for Intramolecular Regulation of Protein Function. The presently described differences between the solution structure of BmPBP^A and the BmPBP conformation in the crystal structure of the BmPBP–bombykol complex imply that the previously described pH-dependent conformational change of BmPBP is related to the mechanism of pheromone binding and release. The BmPBP molecular architecture contains a rigid scaffold of the helices α_{3a}, α_4, α_5, and α_6, which is nearly invariant between the free and the ligand-bound protein, whereas the N-terminal decapeptide segment and the C-terminal dodecapeptide segment show extensive conformational changes between the solution structure of BmPBP^A and the crystal structure of the BmPBP–bombykol complex (Fig. 3). An N-terminal helix of residues 1–13 forms one edge of the binding pocket for bombykol in the structure of the complex (14), whereas most of this segment is flexibly disordered in the solution structure of BmPBP^A. A C-terminal helix α_7 occupies the pheromone-binding site in the hydrophobic core of BmPBP^A, whereas this segment is in an extended conformation on the surface of the BmPBP–bombykol complex. These observations explain the absence of pheromone binding at pH values below 5.0 (12) and indicate a likely passage way for the pheromone into its binding site.

Sandler *et al.* (14) proposed that the three residues His-69, His-70, and His-95 might contribute to the pH-dependent conformation change of BmPBP (7). Comparison of BmPBP^A with the protein conformation in the crystal structure of the complex reveals that the histidine side chains are more widely separated in BmPBP^A. This would reduce the charge repulsion resulting from histidine protonation at slightly acidic pH values and could thus destabilize the structure of the bombykol–BmPBP complex (14) in favor of BmPBP^A. If one accepts the hypothesis that the pH near the membrane surface is lower than the pH value of 6.5 measured in the bulk sensillar lymph (27), these structural data would present a rationale for destabilization of the BmPBP–bombykol complex near the membrane-standing pheromone receptor, which would lead to ejection of the ligand and make it available to the receptor.

Overall, the present NMR structure determination of BmPBP^A suggests an intramolecular regulation mechanism of protein function. It offers a plausible view of pheromone uptake, binding, release, and transfer to the membrane-standing receptor by the pheromone-binding protein of *B. mori*, which has long served as a paradigm for insect olfaction (28).

We thank Dr. Jon Clardy for kindly providing the coordinates of the crystal structure of the BmPBP–bombykol complex before release. This work was supported in part by the Schweizerischer Nationalfonds (Project 31.49047.96), the Komission für Technologie und Inovation KTI (Project Nr. 3392.1), and the Japanese Program for Promotion of Basic Research Activities for Innovative Biosciences.

1. Hansson, B. S. (1995) *Experientia* **51,** 1003–1027.
2. Kaissling, K. E., Keil, T. A. & Williams, J. L. D. (1991) *J. Insect Physiol.* **37,** 71–78.
3. Steinbrecht, R. A. (1996) *Ciba Found. Symp.* **200,** 158–174.
4. Pelosi, P. & Maida, R. (1995) *Comp. Biochem. Physiol. B* **111,** 503–514.
5. Prestwich, G. D. (1996) *Bioorg. Med. Chem.* **4,** 505–513.
6. Maida, R., Proebstl, T. & Laue, M. (1997) *Chem. Senses* **22,** 503–515.
7. Damberger, F., Nikonova, L., Horst, R., Peng, G., Leal, W. S. & Wüthrich, K. (2000) *Protein Sci.* **9,** 1038–1041.
8. Prestwich, G. D. (1993) *Protein Sci.* **2,** 420–428.
9. Briand, L., Nespoulous, C., Huet, J. C., Takahashi, M. & Pernollet, J. C. (2001) *Eur. J. Biochem.* **268,** 752–760.
10. Leal, W. S. (2001) *Pure Appl. Chem.* **73,** 613–616.
11. Nagnan-Le Meillour, P., Huet, J. C., Maïbèche, M., Pernollet, J. C. & Descoins, C. (1996) *Insect Biochem. Mol. Biol.* **26,** 59–67.
12. Wojtasek, H. & Leal, W. S. (1999) *J. Biol. Chem.* **274,** 30950–30956.
13. Leal, W. S. (2000) *Biochem. Biophys. Res. Commun.* **268,** 521–529.
14. Sandler, B. H., Nikonova, L., Leal, W. S. & Clardy, J. (2000) *Chem. Biol.* **7,** 143–151.
15. Bartels, C., Xia, T. H., Billeter, M., Güntert, P. & Wüthrich, K. (1995) *J. Biomol. NMR* **6,** 1–10.
16. Horst, R., Damberger, F., Peng, G., Nikonova, L., Leal, W. S. & Wüthrich, K. (2001) *J. Biomol. NMR* **19,** 79–80.
17. Güntert, P., Mumenthaler, C. & Wüthrich, K. (1997) *J. Mol. Biol.* **273,** 283–298.
18. Nilges, M., Macias, M. J., O'Donoghue, S. I. & Oschkinat, H. (1997) *J. Mol. Biol.* **269,** 408–422.
19. Güntert, P., Billeter, M., Ohlenschläger, O., Brown, L. R. & Wüthrich, K. (1998) *J. Biomol. NMR* **12,** 543–548.
20. Luginbühl, P., Güntert, P., Billeter, M. & Wüthrich, K. (1996) *J. Biomol. NMR* **8,** 136–146.
21. Koradi, R., Billeter, M. & Güntert, P. (2000) *Comput. Phys. Commun.* **124,** 139–147.
22. Cornell, W. D., Cieplak, P., Bayly, I., Gould, I. R., Merz, K. M., Ferguson, D. M., Spellmeyer, T. M., Caldwell, J. W. & Kollman, P. A. (1996) *J. Am. Chem. Soc.* **118,** 2309–2309.
23. Rost, B. & Sander, C. (1993) *J. Mol. Biol.* **232,** 584–599.
24. Wishart, D. S., Bigam, C. G., Yao, J., Abildgaard, F., Dyson, J. H., Oldfield, E., Markley, J. L. & Sykes, D. (1995) *J. Biomol. NMR* **6,** 135–140.
25. Leal, W. S., Nikonova, L. & Peng, G. H. (1999) *FEBS Lett.* **464,** 85–90.
26. Koradi, R., Billeter, M. & Wüthrich, K. (1996) *J. Mol. Graphics* **14,** 51–55.
27. Kaissling, K. E. & Thorson, J. (1980) in *Receptors for Neurotransmitters, Hormones and Pheromones in Insects*, eds. Sattelle, D. B., Hall, L. M. & Hildebrand, J. G. (Elsevier, Amsterdam), pp. 261–282.
28. Schneider, D. (1986) in *Mechanisms in Insect Olfaction*, eds. Payne, T. L., Birch, M. C. & Kennedy, C. E. J. (Clarendon, Oxford, U.K.), pp. 189–191.
29. Morris, A. L., MacArthur, M. W., Hutchinson, E. G. & Thornton, J. M. (1992) *Proteins* **12,** 345–364.